# Theory of physical aging in polymer glasses

Kang Chen and Kenneth S. Schweizer*
*Department of Materials Science and Frederick Seitz Materials Research Laboratory, University of Illinois, 1304 West Green Street, Urbana, Illinois 61801, USA*

(Received 10 January 2008; revised manuscript received 13 August 2008; published 18 September 2008)

A statistical segment scale theory for the physical aging of polymer glasses is proposed and applied. The approach is based on a nonlinear stochastic Langevin equation of motion and the concept of an effective free energy which quantifies temporary localization, collective barriers, and the activated segment hopping process. The key collective structural variable that plays the role of the dynamic order parameter for aging is the experimentally measurable nanometer and longer wavelength amplitude of density fluctuations, $S_0$. The degree of local cooperativity, and the bare activation energy of the high-temperature Arrhenius process, are determined in the molten state by utilizing experimental measurements of the glass temperature and dynamic crossover time, respectively. A first-order kinetic equation with a time varying rate is proposed for the temporal evolution of $S_0$ which is self-consistently and nonlinearly coupled with the mean segmental relaxation time. The theory has been applied to study physical aging of the $\alpha$ relaxation time, shear relaxation modulus, amplitude of density fluctuations, cohesive energy, absolute yield stress, and fictive temperature of polymethylmethacrylate and other glasses over a range of temperatures. Temperature-dependent logarithmic and effective power-law aging is predicted at intermediate times. Time-aging time superposition is found for the mechanical relaxation function. A strongly asymmetric aging response is predicted for up and down temperature jump experiments. Comparison of the approach with the classic phenomenological model is presented.

DOI: 10.1103/PhysRevE.78.031802 PACS number(s): 61.25.H−, 81.40.Cd, 64.70.Q−

## I. INTRODUCTION

The ultraslow, time-dependent dynamics of glasses is a challenging problem of intense scientific and technological interest for a broad range of amorphous materials, from metals to polymers to colloids [1]. Polymer glasses are one of the most studied classes of disordered solids due to their widespread use as plastics [2]. Upon a thermal quench from the equilibrated cold melt a complex phenomenon known as physical aging occurs. All material properties become time dependent, and there are both universal and system-specific aspects to the polymer aging process [2,3]. Thermodynamiclike properties, such as the volume and enthalpy, decrease with time, while mechanical properties, such as the shear modulus and yield stress, increase with time. To a first approximation the intermediate time evolution is logarithmic, with a temperature- and property-dependent slope. The $\alpha$ relaxation time follows power-law aging, with a temperature-dependent effective exponent [2]. Equilibration is often not experimentally accessible since relaxation times grow explosively as temperature decreases by a small amount. The usage temperatures of polymer glasses are not very far below the glass transition temperature, $T_g$, and hence the physical aging problem is of great practical relevance [2].

The approach to thermal equilibrium is generally "asymmetric" in the sense of depending on whether the aging process corresponds to an up or down temperature jump [4,5]. The question of a property dependence of the equilibration time has been controversial. Recent work suggests essentially identical equilibration times for the volume, enthalpy, and mechanical properties [5,6]. This argues that, to a first approximation, a single generic molecular process, the $\alpha$ or structural relaxation, controls all observables [1].

Due to the complexity of the glassy dynamics problem, the vast majority of theories for physical aging are phenomenological and characterized by many adjustable fit parameters of often unclear physical significance [7,8]. Perhaps the most famous in the context of polymer glasses is the Tool-Narayanaswamy-Moynihan (TNM) model [9], which can provide good fits of some experimental measurements. An exception to the phenomenological aspect is the recent work of Lubchenko and Wolynes [10] who have generalized the modern entropy-crisis mean-field approach, the "random first-order phase transition" (RFOT) theory [11], to address the physical aging of polymers. The RFOT analysis has provided microscopic insight to the prior phenomenological approaches, and is consistent with established connections between the dynamic fragility and the so-called nonlinearity parameter.

Computer simulations of the aging of glassy polymers have been recently performed [12,13]. A key finding is that the consequences of aging for macroscopic quantities (e.g., creep compliance) are consistent with microscopic dynamics, e.g., segmental mean-square displacement or incoherent dynamic structure factor on the cage scale [13]. This is significant since creep involves collective mechanical and structural relaxation, but nevertheless is closely correlated with the conceptually much simpler self-dynamics of single segments. Moreover, aging processes appear to be controlled by elementary activated motions on a relatively small length scale, a feature that provides the foundation for our theoretical approach to the problem.

Recently, Saltzman and Schweizer have constructed and applied a force level theory for activated barrier hopping segmental dynamics in equilibrated cold polymer melts [14,15]. The approach was generalized to the nonequilibrium

*kschweiz@uiuc.edu

 

glass state in the absence of aging by the present authors [16]. In a recent paper the extension of this theory to treat physical aging was reported [17], and encouraging comparisons to experiment were demonstrated. The goal of the present paper is to present a detailed account and application of our theory of polymer physical aging. Features not previously addressed include the aging of the enthalpy, shear elastic modulus and yield stress, the role of nonexponential relaxation, the asymmetry between up and down temperature jump experiments, fictive temperature, time-aging time superposition of stress relaxation, and consideration of alternative formulations of the nonequilibrium equation of motion for the primary structural variable.

Section II summarizes the key elements of the theory for quiescent melts and glasses. A discussion of the mapping from the atomistic to segment level is given in Appendix A. The aging theory is described in Sec. III, and a statistical mechanical motivation is presented in Appendix B. Comparison of the essential elements of the approach to a popular phenomenological model is the subject of Appendix C. Section IV presents model calculations for a wide range of phenomena. An alternative version of the theory is given in Sec. V and its consequences briefly explored. Section VI presents quantitative comparisons of the theory with measurements of various properties of polymethymethacrylate (PMMA) glass. The paper concludes in Sec. VII with a discussion.

## II. THEORETICAL BACKGROUND

Our theory for physical aging is built on work discussed in depth previously for quiescent supercooled polymer melts and glasses [14–17]. In this section the key elements are summarized.

### A. Equilibrium cold melt

An atomistic, first principles theoretical description of the dynamics of polymer melts is intractable. Hence, in the spirit of essentially all theories of polymer dynamics [18], the melt is treated as a liquid of lightly coarse-grained "statistical segments" of size $\sigma$. To a first approximation the dynamical consequences of chain connectivity beyond the segment scale are ignored. This simplification is globally justified since glassy dynamics becomes chain length independent for long polymers [19]. Of course, material-specific local chain structure (backbone stiffness, monomer shape) is quantitatively important, but is very difficult to treat. Hence, we adopt the simplest "Gaussian thread chain" model defined entirely by the segment length and degree of polymerization, $N$ [14].

The essence of the theory is a closed nonlinear stochastic Langevin equation of motion for the instantaneous scalar displacement of a segment from its initial ($t=0$) location, $r(t)$. In the overdamped, high friction regime of interest it is given by [14,20]

$$-\zeta_s \frac{\partial r(t)}{\partial t} - \frac{\partial F_{\rm eff}[r(t)]}{\partial r(t)} + \delta f(t) = 0, \tag{1}$$

where the white-noise random force satisfies $\langle \delta f(0)\delta f(t)\rangle = 2k_BT\zeta_s\delta(t)$, and $\zeta_s$ is a friction constant that describes very local, short-time irreversible dynamics. The "nonequilibrium free energy" consists of ideal entropy and caging contributions

$$\beta F_{\rm eff}(r) = -3\ln(r) - \int \frac{d\mathbf{q}}{(2\pi)^3}\rho C^2(q)S(q)[1+S(q)]^{-1} \times \exp\left(-\frac{q^2r^2}{6}[1+S^{-1}(q)]\right), \tag{2}$$

where $C(q)$ is the Fourier transform of the site-site intermolecular direct correlation function, $S(q)$ is the dimensionless collective density fluctuation structure factor, and $\beta \equiv (k_BT)^{-1}$. The physical basis [14,15] and statistical mechanical derivation [20] of the theory has been discussed. The key idea is to use time-dependent density functional methods at the dynamical variable level, in conjunction with a local equilibrium picture and a self-consistent approximate relation between one and two particle dynamics. Equation (1) can be viewed as in the spirit of model A for a nonconserved dynamic order parameter [20,21] with the key difference that $F_{\rm eff}$ is not an equilibrium free energy.

The Gaussian thread chain model has been extensively discussed in the context of polymer integral equation theory [22]. The idea is to coarse grain over the local Ångstrom-scale single-chain structural and interaction potential length scales. As described previously [14,22], and in depth in Appendix A in the context of the dynamical theory, the structural consequences of this coarse graining are that the site-site direct correlation function becomes wave-vector independent, $C(q)=C_0$, and a simple Lorentzian form for the collective static structure factor applies, $S^{-1}(q)=S_0^{-1}+(q\sigma)^2/12$. Here, $S_0 \equiv S(q=0)=\rho k_BT\kappa=(-\rho C_0)^{-1}\propto\langle(\delta\rho)^2\rangle$ is the dimensionless compressibility, which quantifies the amplitude of nanometer and beyond thermal number density fluctuations. This quantity plays the role of the primary structural variable, or dynamic order parameter, since the starting point of the theory is the mode coupling approach based on collective density fluctuations as the key slow variable. Since coarse graining to the segment level involves removing degrees of freedom, the statistical segment length cannot be uniquely determined. However, for Gaussian chains the intrapolymer equilibrium pair correlations are uniquely specified [14] by a segment of size $\sigma=\sqrt{C_\infty}l$, where $l$ is the mean backbone chemical bond length and $C_\infty$ is the characteristic ratio. The dimensionless melt density, $\rho\sigma^3$, is of order unity.

As discussed previously [14,22] and in Appendix A, coarse graining to the nanometer segmental scale results in the removal of the wide angle (peak) scattering features in $S(q)$. It is also important to appreciate that a literal $q\to 0$ approximation is not being invoked. The quantity $S_0$ emerges as the key variable since on the segmental scale the low amplitude collective density fluctuations of real polymer melts are to a very good approximation homogeneous in the sense $S(q)$ is constant on $q\sigma<1$ scales [22].

Using the above results, simple algebra and appropriate nondimensionalizations allow the nonequilibrium free energy to be written as [14]

$$\beta F_{\rm eff}(\alpha^*) = \frac{3}{2}\ln(\alpha^*) - \frac{12\sqrt{3}}{\pi}\lambda\int_0^\infty dy\left(\frac{y}{1+y^2}\right)^2 \times \exp\left(-\frac{y^2(1+y^2)}{4\alpha^*}\right)$$

$$\lambda \equiv \frac{1}{\rho\sigma^3 S_0^{3/2}}, \tag{3}$$

where $y \equiv q\sigma\sqrt{S_0/12}$, $\alpha \equiv 3/2r^2$ and $\alpha^* \equiv \alpha\sigma^2 S_0^2/12$. As true for hard sphere and small molecule systems [23,24], the intermolecular force (caging) contribution to the effective free energy is controlled by "large" $q\sigma > 1$ wave vectors. This point is carefully explained in Appendix A. The theory is characterized by a dimensionless "coupling constant," $\lambda$, determined by experimentally measurable equilibrium quantities. Minimization of the nonequilibrium free energy with respect to $r$, or dropping the thermal noise term in Eq. (1), yields a self-consistent localization equation for the "naïve" mode coupling theory (MCT) ideal glass or nonergodicity transition [25,26] which occurs at $\lambda_c = 8.32$ and a corresponding temperature $T_c$. Polymer integral equation theory suggests a simple temperature dependence for $S_0$ which has been demonstrated to describe experimental data extremely well [14],

$$S_0^{-1/2} = -A + (B/T), \tag{4}$$

where $A > 0$ and $B$ is related to the melt cohesive energy and correlates with polymer polarity. Combining Eqs. (3) and (4), and taking the segmental density as a material constant, yields

$$T_c = \frac{B}{A + (\lambda_c \rho\sigma^3)^{1/3}}. \tag{5}$$

If thermally driven barrier hopping is ignored, then this $T_c$ represents the ideal (naïve) MCT glass transition temperature. In our approach, below $T_c$ ($\lambda > \lambda_c$) there is a smooth crossover to the deeply supercooled regime where collective barriers due to segment-segment interchain forces emerge. The nonequilibrium free energy is then characterized by a metastable local minimum and a barrier of height $F_B$. Numerical calculations find that the barrier is extremely well described by a critical power-law form [14],

$$\beta F_B \approx c(\lambda - \lambda_c)^\Delta, \quad c \cong 0.4, \quad \Delta \simeq 1.3. \tag{6}$$

Consistent with experiment, above $T_c$ the dynamics is treated in an Arrhenius manner corresponding to a "primitive" $\alpha$ relaxation time $\tau_0(T) \equiv \tau_0 \exp(\varepsilon/k_B T)$, where $\tau_0 \approx 10^{-14\pm1}$ s is a vibrational time scale and $\varepsilon$ is a material specific local activation energy. The simplest model for the mean hopping ($\alpha$) time that smoothly bridges the normal and supercooled regimes is employed [14,15],

$$\tau_\alpha(T) = \tau_0 \exp\left(\frac{\varepsilon}{k_B T}\right)\exp\left(\frac{a_c F_B(T)}{k_B T}\right). \tag{7}$$

Equation (7) corresponds to adopting the primitive $\alpha$ time as the dynamical prefactor (attempt time scale) for barrier hopping, and detailed discussion of the approximations underlying it has been given [14,15]. Briefly, Eq. (7) has not been rigorously derived from Eqs. (1) and (2), but rather encodes the key elements of a high-temperature Arrhenius process and the crossover to strongly activated non-Arrhenius relaxation below $T_c$. A MCT-like critical power-law type of temperature dependence is often present over a narrow intermediate temperature region that corresponds to a few orders of magnitude in relaxation time [1]. For simplicity, this aspect has been ignored in Eq. (7) since our focus is the deeply supercooled melt and the below $T_g$ glass regimes where traditional mode-coupling effects are not relevant.

In reality there are short-range equilibrium correlations between connected segments that have dynamic consequences. To model this a temperature-independent, but polymer-specific, cooperativity parameter, $a_c$, is introduced which leads to an effective barrier height of $a_c F_B$. Physically, $a_c$ corresponds to the number of dynamically correlated segments along the chain and its magnitude is determined by an intramolecular correlation length. It is well known in polymer physics that the "dynamical" segment length is not the same as its analog that describes equilibrium single-chain correlations [27,28]. The dynamical segment length is typically estimated from a measure of chain stiffness: Either the Kuhn length $l_K = C_\infty l$, or persistence length $\xi_p = (C_\infty + 1)l/2$ [18], thereby yielding $a_c = C_\infty$ or $a_c = (C_\infty + 1)^2/4C_\infty$, respectively [15]. Given $C_\infty \approx 4-10$, one finds $a_c \sim 1-10$. For PMMA, since $C_\infty \sim 9$ and $l \sim 0.15$ nm, the equilibrium and dynamic estimates of a segment length lie in the range of $\sim 0.5-1.5$ nm [15,16]. We note that our treatment of local chain stiffness on the barrier hopping process is not a first principles one, but rather is motivated by physical considerations.

The nonuniversal local activation energy, $\varepsilon$, is not *a priori* known, and is coarse grained over at the segment level. It is determined by adopting the recent proposition [29] of a (nearly) universal "magic relaxation time" at the dynamical crossover given by $\tau_0(T_c) \cong 10^{-7\pm1}$ s. This condition, plus Eq. (3), then yields (for $\tau_0 \approx 10^{-14}$ s) $\varepsilon \cong (16.1 \pm 2.5) k_B T_c$. Equations (3)–(7) constitute the analytic theory for the $\alpha$ time in the deeply supercooled regime. The practical experimental criterion for a glass transition is $\tau(T_g) = 10^x$ s where $x = 2-4$.

The theory focuses on a generic $\alpha$ time and does not distinguish between dielectric, mechanical, light scattering or other specific experimental probes of glassy relaxation. The relaxation times extracted from distinct nondiffusive measurements are very similar in magnitude and temperature dependence [1]. Some insight concerning this issue is given in Appendix B where the low wave-vector collective dynamic structure factor is shown to be closely related to stress relaxation. Our polymer theory at present does not address "dynamic heterogeneity" effects at the segmental scale that result in strong decoupling of translational diffusion constant and viscosity in the deeply supercooled regime of small molecule liquids [29,30]. We note that decoupling of macroscopic transport coefficients does not occur for polymers since the macromolecular size is far larger than any dynamic heterogeneity length scale associated with the fast (relative to chain scale motions) segmental dynamics [31].

Extensive applications of the melt theory to predict the crossover temperature, $T_g$, dynamic fragility, temperature

and pressure dependence of the relaxation time, shear modulus and other aspects have been performed. They provide a consistent picture of segmental dynamics based on a theory with no singularities at nonzero temperature [14,15].

### B. Below the glass transition temperature

Below $T_g$ the fundamental aspects of the theoretical approach are assumed to still apply [16]. The ultralocal fast process is taken to remain in equilibrium, and hence the fluctuation-dissipation relation involving the short-time friction constant in Eq. (1) still holds. In the potential energy landscape (PEL) picture [32], the fast process corresponds to "intrabasin" harmoniclike vibrational motions and small scale relaxation dynamics within a single inherent structure or megabasin. However, structural degrees of freedom, the relaxation of which define the slow $\alpha$ process, fall out of equilibrium. As discussed theoretically [16] and experimentally [33], the statistical mechanical relationship $(-\rho C_0)^{-1}=S(q=0)=\rho k_B T\kappa$ between the amplitude of density fluctuations and isothermal compressibility no longer holds. In our theory the key structural variable remains $S_0$, which must be interpreted as quantifying nanometer and longer wavelength density fluctuations. In the PEL picture the sub-$T_g$ dynamics exhibits aging since the system is trapped in higher energy inherent structures on the experimental time scale [32]. The aging process corresponds to a slow approach to equilibrium via the exploration of deeper states on the landscape which lower potential energy.

The density fluctuations that enter $S_0$, and hence the coupling constant $\lambda$, contain an equilibrated part associated with the fast intrabasin dynamics. We model this contribution as linear in temperature, which is an exact description for an idealized harmonic crystal [34]. In the initial (preaging) out-of-equilibrium state the diverse packing arrangement contribution to $S_0$ is taken to be frozen at a level that corresponds to its equilibrated value at $T_g$. In the absence of physical aging this contribution persists to zero Kelvin. Its magnitude is modeled via a single material constant, $b$, defined as the fraction of $S_0(T=T_g)$ unrelaxed at $T=0$. The physical aging process then corresponds to the time evolution of this frozen part back to its equilibrium value as defined via extrapolation of the equilibrium $S_0(T)$ curve below $T_g$. The elementary landscape arguments given above, and small angle scattering measurements on many polymer glasses [33], motivate a simple additive description of the structural and vibrational contributions [16],

$$S_0(T) \simeq bS_0(T_g) + (T/T_g)(1-b)S_0(T_g), \tag{8}$$

where $S_0(T\to 0)\equiv bS_0(T_g)$. Scattering measurements [33,35] suggest the polymer-specific parameter $b\sim 0.5-0.75$, corresponding to the structural component comprising $\sim 50\%-75\%$ of the total density fluctuation amplitude at $T_g$. This range of the parameter $b$ is consistent with the typical drop by a factor of 2–3 of the isothermal compressibility at the glass transition [33].

Calculations of the $\alpha$ relaxation time for polymethylmethacrylate (PMMA) are shown in Fig. 1 based on the identical parameters employed in previous work [16,17,36].

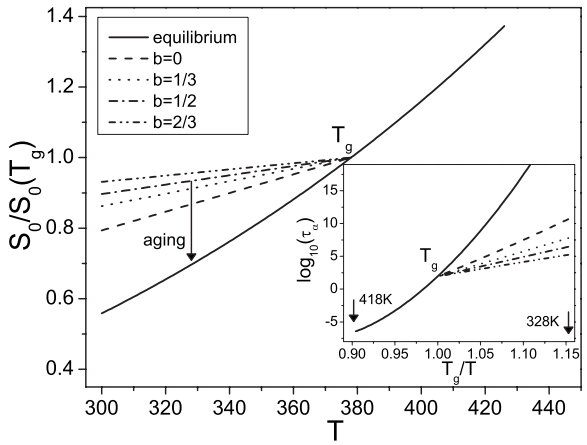


FIG. 1. Main panel: Schematic of the aging process in terms of $S_0$. Normalized $S_0(T)$ as a function of temperature (Kelvin) for parameters relevant to PMMA [16] ($A=0.693$, $B=1134$ K, $\rho\sigma^3=0.92$, $a_c=5$, $T_g=378$ K, $T_c=426$ K, $\tau_\alpha(T_g)=100$ s) and several values of $b$ in Eq. (4). The inset shows the crossover to an apparent Arrhenius behavior of the mean relaxation time below the glass transition temperature.

In many cases measurements are performed rapidly ("quenching") and aging is minimal. Under this condition an effective Arrhenius behavior is generically obtained [16] (inset of Fig. 1), and our results are in good agreement with many measurements [37]. The physical picture is the Arrhenius temperature dependence is a consequence of the solid-state-like thermal dependence of the amplitude of nanometer and longer wavelength density fluctuations.

## III. THEORY OF PHYSICAL AGING

As indicated in the main panel of Fig. 1, the aging process corresponds to an evolution of the amplitude of density fluctuations from its nonequilibrium $t=0$ value given by Eq. (8) to the smaller long-time equilibrium value, $S_{0,l}$. In the landscape picture the reduction of the inherent structure potential energy and exploration of deeper states corresponds to a decrease of liquid disorder and hence a lower $S_0$. The local fast process is taken to be unaffected by physical aging. Such a simplification is not exact, but generally quite accurate [2,38]. The collective barrier and mean hopping time become time dependent via $S_0(t)$ [39].

We postulate a first-order kinetic model for the aging of the dynamic order parameter

$$\frac{dS_0(t)}{dt} = -\frac{S_0(t)-S_{0,l}}{\tau_\alpha[\lambda(t)]}. \tag{9}$$

Here, $S_{0,l}$ is the equilibrated value of $S_0$, and $\lambda(t)$ is the quantity defined in Eq. (3) where the time dependence arises solely from the aging of $S_0$. Equation (9) corresponds to the self-consistent idea that the time evolution of density fluctuations is driven by segmental barrier hopping which itself is determined by $S_0(t)$ via Eqs. (3), (6), and (8). A statistical mechanical motivation for Eq. (9) is given in Appendix B. Many "first-order" kinetic aging equations have appeared in

the literature [1,7,8]. However, they are generally based on phenomenological, difficult to quantify concepts such as a fictive temperature or "free volume." We emphasize that Eq. (9) involves the measurable amplitude of density fluctuations and is devoid of adjustable parameters. The relationship of our theory for glass relaxation and aging to the commonly applied phenomenological model is discussed in Appendix C.

The formal solution of Eq. (9) is

$$S_0(t) = S_{0,l} + (S_{0,g} - S_{0,l})e^{-\int_0^t [dt'/\tau_\alpha(t')]}, \tag{10}$$

where $S_0(t=0)=S_{0,g}$ is the $t=0$ unaged value after a quench described by Eq. (8). Equation (10) is of an "effective time" form, which can equivalently be written in a normalized manner as

$$\frac{S_0(t) - S_{0,l}}{S_0(0) - S_{0,l}} = e^{-\int_0^t [dt'/\tau_\alpha(t')]}. \tag{11}$$

Equation (9) is a single relaxation time, time local description. Its temporal locality is consistent with the "local equilibrium" idea underlying the effective free energy and stochastic nonlinear Langevin equation [19] used to describe the supercooled melt dynamics. Dynamic heterogeneity [29] associated with a distribution of relaxation times is ignored. However, (weak) nonexponential time evolution does occur due to the time-dependent relaxation time. Given $\lambda(t) \equiv [\rho\sigma^3 S_0^{3/2}(t)]^{-1}$ and Eqs. (3) and (7), Eq. (9) is a self-consistent, highly nonlinear description of the aging dynamics of $S_0(t)$ and relaxation time. Combining Eqs. (6), (7), and (10) yields an explicit integral equation for the time-dependent $\alpha$ relaxation time

$$\tau_\alpha(t) = \tau_0(T)\exp\left[ ca_c\left(\left\{ \rho\sigma^3\left[ S_{0,l} + (S_{0,g} - S_{0,l}) \times\exp\left( -\int_0^t dt'\,\tau_\alpha^{-1}(t') \right) \right]^{3/2} \right\}^{-1} - \lambda_c \right)^{\Delta} \right]. \tag{12}$$

## IV. RESULTS

We now apply the theory of Secs. II and III using the same PMMA parameters as in previous work [17]. It is important to summarize how the material parameters are chosen [16,17] and what is, and is not, adjusted. First, the glass transition temperature is fixed by the kinetic criterion that the $\alpha$ time at $T_g$ equals 100 s. The cooperativity parameter is chosen as $a_c=5$ in order to reproduce a representative value of $T_g=378$ K for PMMA. This value of cooperativity parameter lies in between the *a priori* estimates of $a_c=3$ and 9 based on adopting the persistence or Kuhn length, respectively, as a measure of dynamic stiffness [15,16]. Moreover, $a_c=5$ leads to a predicted dynamic fragility at $T_g$ in excellent agreement with experiment [16]. The bare Arrhenius activation energy, $\varepsilon$, is fixed from the experimental dynamic crossover time and our theoretical computed $T_c$. In quantitative applications to PMMA the dimensionless segmental density, $\rho\sigma^3$, is adjusted so that the theoretical $T_c$ of Eq. (5) equals its experimentally estimated analog [16]. It is important to emphasize that all these material parameters are determined from the equilibrium melt state behavior of PMMA, and none are varied as fit parameters in our study of physical aging in the glass. Finally, in the glass state only one additional parameter enters: $b$ in Eq. (8), which quantifies the amplitude of frozen density fluctuations. For PMMA this parameter is fixed at $b=2/3$ as suggested by x-ray scattering measurements [33,35]. In some plots we vary $b$ in order to illustrate the sensitivity of our results to this parameter.

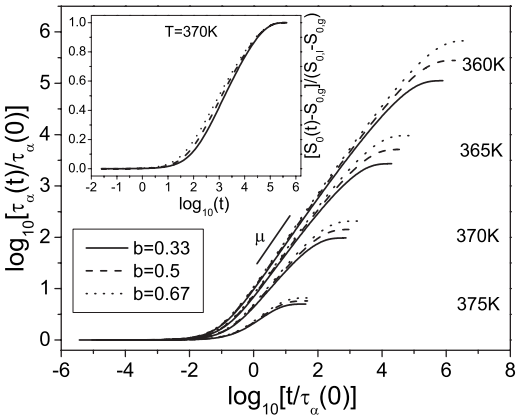


FIG. 2. Doubly normalized log-log plot of the relaxation time for several values of $b$ and different cooling depths. The evolution of $S_0$ at 370 K in the representation of Eq. (11) is shown in the inset.

### A. Effective aging exponent for the relaxation time

Calculations of the time evolution of the structural variable $S_0(t)$ at 8 K below $T_g$ are shown in the inset of Fig. 2. As experimentally observed for essentially all properties, the basic shape of the aging curve is sigmoidal [3]. Consistent with measurements of the density, shear modulus, and enthalpy, the intermediate time behavior is roughly logarithmic. The shape shows a weak dependence on the fraction of frozen in density fluctuation parameter, $b$.

The time evolution of the $\alpha$ time for various cooling depths is also shown in Fig. 2 in a doubly normalized log-log plot. The curves are again sigmoidal. The equilibration time (plateau) increases extremely rapidly with cooling, and is found to be roughly equal to the $\alpha$ time of the equilibrium supercooled melt. A good power-law behavior, $\tau_\alpha(t) \propto t^\mu$, occurs at intermediate times which depends strongly on temperature and weakly on the parameter $b$. An apparent aging exponent, $\mu = d\ln[\tau_\alpha(t)]/d\ln(t)$, can be accurately extracted.

The inset of Fig. 3 shows the aging exponent initially increases sharply with cooling below $T_g$, and then slowly approaches unity from below. Note the almost complete insensitivity of the temperature dependence of the aging exponent on the parameter $b$. The time axis in Figs. 2 and 3 are scaled by the initial relaxation time, and $\mu$ is determined under the assumption that all time scales are accessible. However, as discussed previously [17], only a limited time window can be accessed in experiment which we suggest is

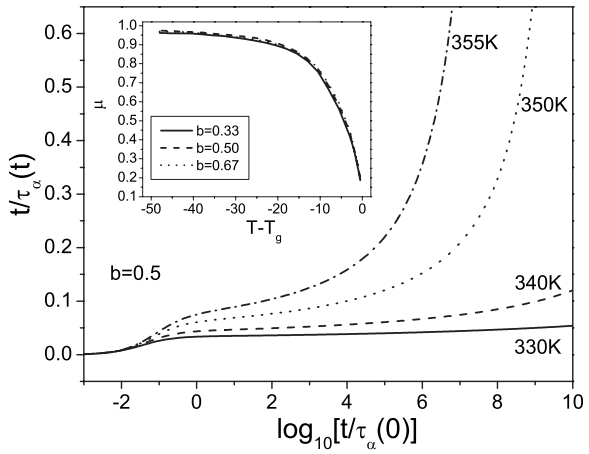


FIG. 3. Time-dependent ratio $t/\tau_\alpha(t)$ at several temperatures. A plateau emerges at intermediate time. The inset shows the apparent aging exponent as a function of cooling depth.

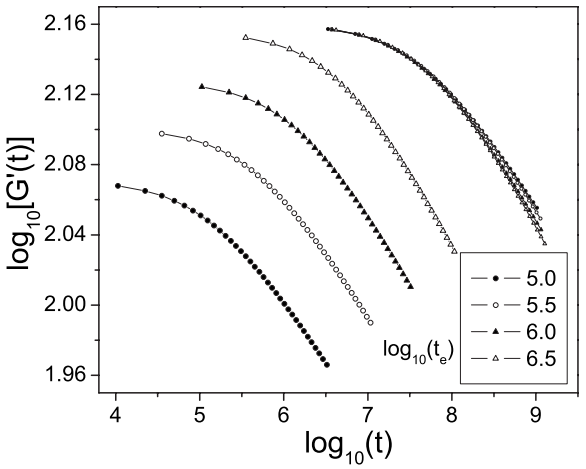


FIG. 4. Time-dependent stress relaxation modulus corresponding to four different aging times ($t_e$) and $T=350$ K, $b=0.5$. The master curve constructed by vertical and horizontal shifting is shown in the upper right.

the origin of the nonuniversal downturn of $\mu(T)$ at low temperature observed [2] in polymer glasses.

Mathematically, our predictions for the aging exponent follow from the fact that $\mu=d(\beta a_c\{F_B[\lambda(t)]-F_B[\lambda(0)]\})/d\ln(t)$ is determined by the time evolution of the barrier. The latter depends on the magnitude and time dependence of $S_0(t)$ which at intermediate times decreases roughly linearly with $\ln(t)$ (inset in Fig. 2) and $d[dS_0(t)/d\ln(t)]/dt\approx 0$. Using this condition, Eq. (9), and the definition of the aging exponent, one can show that $\mu=1-t/\tau_\alpha(t)$ evaluated in the intermediate time regime. Figure 3 demonstrates that this quantity is roughly constant in this regime, i.e., $t/\tau_\alpha(t)$ is nearly constant and decreases with cooling resulting in a monotonic increase of $\mu\to 1$. Moreover, $\mu$ is bounded from above by unity; although we do not know of a fundamental reason, this must be the case in our theory. The precise value of $T_g-T$ where the exponent tends to saturate depends on polymer and sometimes the method of measurement [2]. However, the large majority of experiments suggest the effective exponent does not exceed unity, although a few exceptions apparently exist [2].

### B. Shift factor and time-aging time superposition

Many polymer aging experiments do not directly measure the time-dependent relaxation time, but rather deduce it by constructing master curves of creep [2] and stress relaxation mechanical data [40] via a superposition procedure. The measured shift factor, $a_{t_e}(t_e,t_e^{\rm ref})\equiv\tau_\alpha(t_e)/\tau_\alpha(t_e^{\rm ref})$, reflects the change of the characteristic relaxation time with aging time, $t_e$, relative to a "reference" state which aged a time $t_e^{\rm ref}$. To mimic such an experiment we calculate the shear stress relaxation modulus, $G(t)$. In analogy with our treatment of $S_0(t)$, and motivated by Appendix B, a simple exponential-like form is employed

$$G(t_e+t)=G'(t_e)\exp\left(-\int_{t_e}^{t_e+t}\tau_\alpha^{-1}(t')dt'\right), \qquad (13)$$

where $G'(t_e)$ is the glassy modulus calculated using the Green-Kubo formula [41,42]

$$G'=\frac{k_BT}{60\pi^2}\int_0^\infty dq\left(q^2\frac{\partial}{\partial q}\ln S(q)\right)^2 e^{-q^2r_L^2/3S(q)}. \qquad (14)$$

The shear modulus is determined by the time-dependent density fluctuation amplitude and localization length $r_L$.

The shear stress relaxation curves as a function of aging time for different waiting times are shown in Fig. 4 on an expanded scale as employed in experimental studies [2,40]. By performing a horizontal shift [vertical shift is fixed by $G'(t_e)$], a good master curve can be constructed. We find (not plotted) that the aging time dependence of the horizontal shift factor, and the directly computed normalized relaxation time, are in nearly perfect agreement.

### C. Aging of cohesive energy, elastic modulus, and yield stress

It is well established that thermodynamic, relaxation, and mechanical properties all change with time during physical aging. Possible quantitative differences of their aging behavior is of interest. Based on the Gaussian chain model, polymer integral equation theory [22] for the site-site interchain pair correlation function, $g(r)$, and a Yukawa form of the attractive site-site potential, $v(r)$, it has been shown that the cohesive energy density is [14]

$$U_{\rm coh}=\frac{1}{2}\rho^2\int d\mathbf{r}\,v(r)g(r)=-2\pi\rho^2a^3\varepsilon\left(1+\frac{\sigma}{a}\sqrt{\frac{S_0}{12}}\right)^{-1}, \qquad (15)$$

where $v(r)=-\varepsilon a r^{-1}e^{-r/a}$ is the site-site interchain attraction of range $a$ and strength $\varepsilon$. The effect of deformation on the nonequilibrium free energy and barrier hopping process has been discussed in detail [36,43]. The basic idea is that stress results in a mechanical work-type contribution to the nonequilibrium free energy in Eq. (2), which increases the localization length and reduces the barrier. The absolute yield stress, $\tau_{\rm abs}$, is the minimum stress required to destroy the barrier and transform $F_{\rm eff}(r)$ to a monotonically decaying

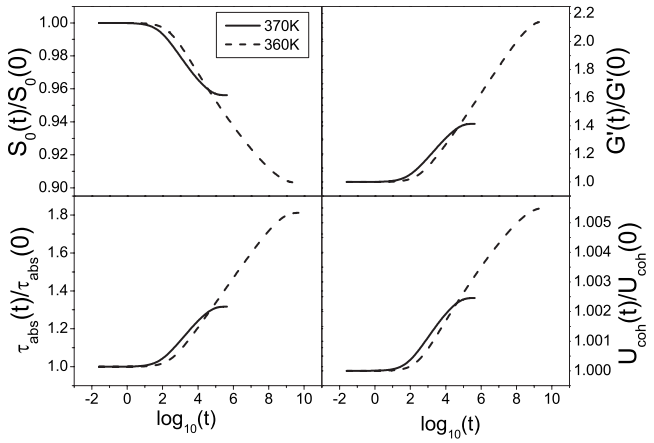


FIG. 5. Aging of the $S_0$, elastic modulus $G'$, absolute yield stress $\tau_{abs}$, and cohesive energy $U_{coh}$ ($\sigma=a$) at two temperatures 370 K and 360 K, and $b=0.5$.

delocalized form. In the absence of noise this corresponds to a mechanically induced devitrification transition.

Figure 5 shows the normalized time evolution curves of the long wavelength density fluctuation amplitude, elastic modulus, cohesive energy, and absolute yield stress. The relative changes are property specific. For example, at 360 K, $S_0$ decreases by $\sim 10\%$, the modulus and absolute yield stress increase by $\sim 75\% - 100\%$, and the cohesive energy changes by $<1\%$. These differences reflect the fact that distinct properties have differing sensitivities to the density fluctuation amplitude. The shape of all aging curves are sigmoidal with roughly logarithmic behavior at intermediate times. The final and initial values differ more at lower temperature.

Figure 6 presents the same calculations but in a normalized format. All properties age quite similarly near $T_g$, and almost collapse onto a master curve. But at lower temperature significant differences emerge at intermediate times with $S_0$ and cohesive energy varying more rapidly, and then more slowly at longer times, compared to the mechanical properties. The absolute yield stress and modulus follow a uniform logarithmic behavior at all intermediate times.

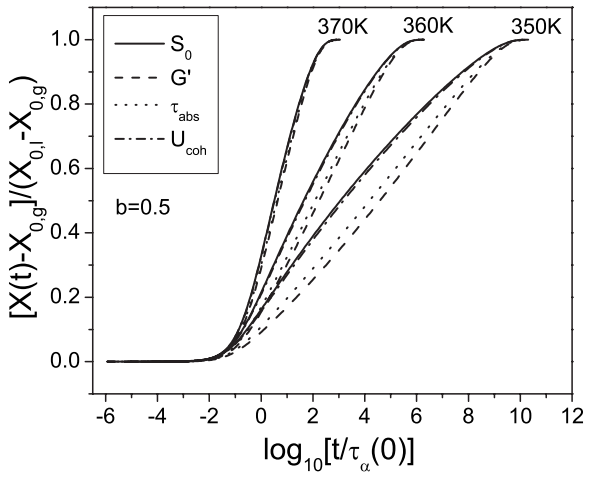


FIG. 6. Normalized aging plot of the four quantities in Fig. 5: $S_0$ (solid line), $G'$ (dashed line), $\tau_{abs}$ (dotted line), and $U_{coh}$ (dashed-dotted line).

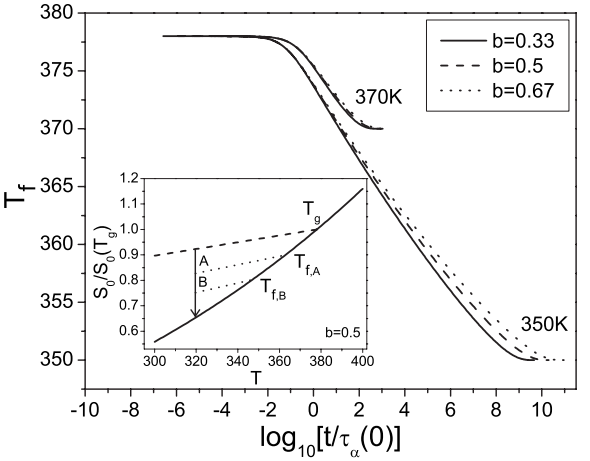


FIG. 7. Main panel: Time evolution of the fictive temperature at two temperatures and three $b$ values. Inset: Schematic of the rule for determination of the fictive temperature.

### D. Fictive temperature

The fictive temperature $T_f$ is traditionally defined as the temperature at which the liquid structure is frozen when cooling through the glass transition [9]. The inset of Fig. 7 shows the procedure for its determination in our approach, which quantifies the extent of equilibration of the structural (megabasin) contribution to density fluctuations. Specifically, the nonequilibrium glass state has the same frozen long wavelength density fluctuation as the corresponding equilibrium state at $T_f$ [44]. Freshly quenched states have the same fictive temperature, $T_g$. As aging progresses, $T_f$ decreases and becomes the real temperature in the long time limit.

The main panel of Fig. 7 presents fictive temperature calculations starting from freshly quenched states of 370 K and 350 K for three values of the frozen density fluctuation parameter, $b$. Similar to the behavior of thermodynamic and mechanical quantities, the fictive temperature varies in a roughly logarithmic manner at intermediate times which depends slightly on $b$.

### E. Up versus down temperature jump experiments

A schematic of the up and down temperature jump experiment is shown in Fig. 8. It is assumed that the intrabasin or phononlike contribution to the long-wavelength density fluctuation amplitude changes instantaneously with temperature jump, and that Eq. (9) is available for describing the evolution of the frozen part of density fluctuation for the up-jump experiment.

Figure 9 and its inset show the evolution of the $\alpha$ relaxation time and $S_0$, respectively, for jump temperatures depicted in Fig. 8. In qualitative agreement with experiment [4,5], the strong asymmetry at fixed temperature jump magnitude, $\Delta T$, is evident. For the up-jump process there is an extremely long initial plateau which extends further for lower initial temperature and accounts for the longer equilib-

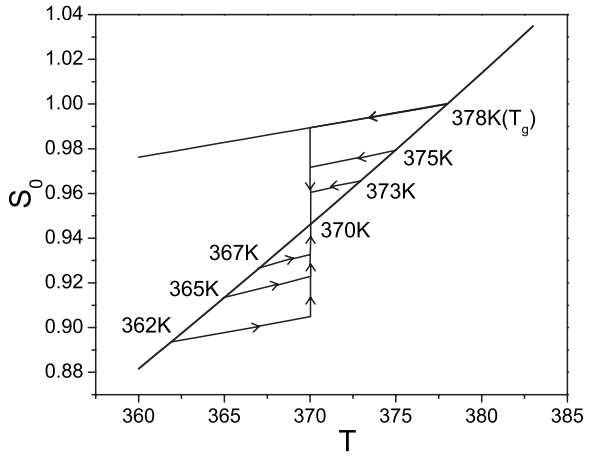


FIG. 8. Schematic of the up- and down-jump experiments and at the temperatures studied.

rium time. However, the evolution rate (absolute slope of the curve) in the following intermediate time regime is much quicker than the down-jump process. It is significant to note that the down-jump process follows an intermediate power-law aging behavior, but the up-jump aging process does not, as also found in experiments [3,19].

## V. ALTERNATIVE MODELS

As true of all practical models of physical aging, our nonequilibrium evolution equation for the primary structural variable has been postulated, not derived. A motivation for its form is given in Appendix B. It seems worthwhile to explore different ansatzes to test how sensitive our results are to details of the dynamical description. We also consider at a primitive level the possible role of non-Maxwell model-like, or stretched exponential, description of relaxation.

### A. Time local description

Recently Loidl and co-workers [45] proposed and applied a simple ansatz for the physical aging of molecular glasses.

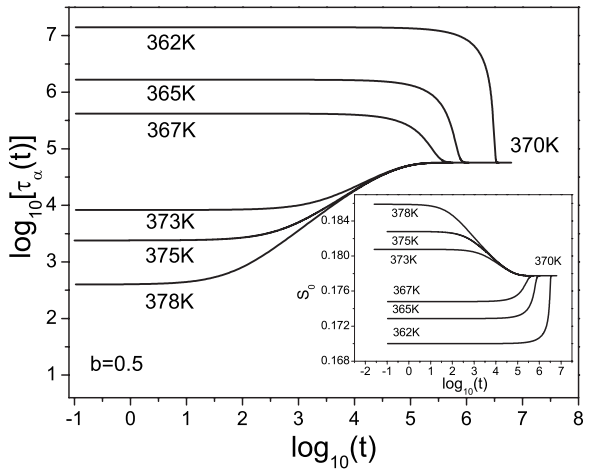


FIG. 9. The aging of the $\alpha$ relaxation time (main panel) and density fluctuation amplitude $S_0$ (inset) corresponding to the up- and down-jump processes in Fig. 8.

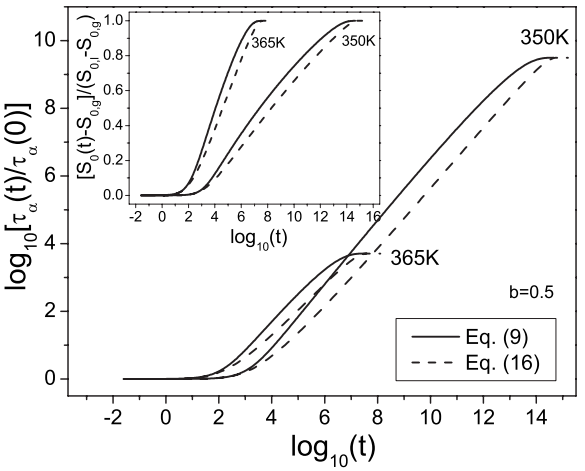


FIG. 10. Comparison of aging predictions of Eq. (9) and Eq. (16): Relaxation time (main panel) and density fluctuation amplitude (inset).

They demonstrated their model could reproduce a variety of dielectric data quite well. In our notation their model, in the Maxwell spirit, is given by

$$S_0(t) = S_{0,l} + (S_{0,g} - S_{0,l})e^{-t/\tau_\alpha(t)}. \tag{16}$$

The time locality of Eq. (16) precludes describing memory effects associated with the coupling of aging and other processes. We have implemented this approach.

The aging of $S_0(t)$ (inset) and the relaxation time (main panel) predicted by Eq. (16) are shown in Fig. 10 and contrasted with results based on Eq. (9). There are no major differences in the shapes of the curves. However, Eq. (16) predicts a slightly slower aging process which can be quantified by calculating the apparent aging exponent as shown in Fig. 12 (solid versus dashed-dotted curves). The aging exponent for both models approach unity at low temperature.

### B. Heterogeneity and nonexponential relaxation

The slow structural $\alpha$ relaxation is generally characterized as nonexponential in time [1] and described by a stretched exponential or Kohlrausch-Williams-Watts (KWW) function. This form mimics, or is a consequence of, a distribution of relaxation times due to dynamic heterogeneity. The latter has not been explicitly taken into account in our approach. To crudely address this issue, we investigate how the predictions of our theory change if the underlying relaxation process is described by a stretched exponential function. Since we assume physical aging proceeds via the $\alpha$ relaxation process, it is natural to incorporate nonexponential relaxation by generalizing Eq. (10) to

$$S_0(t) = S_{0,l} + (S_{0,g} - S_{0,l})e^{-(\int_0^t [dt'/\tau_\alpha(t')])^{\beta_K}}, \tag{17}$$

where $\beta_K$ is the KWW stretching exponent which is taken to be temperature independent. Differentiating Eq. (17) with respect to time yields the corresponding differential form

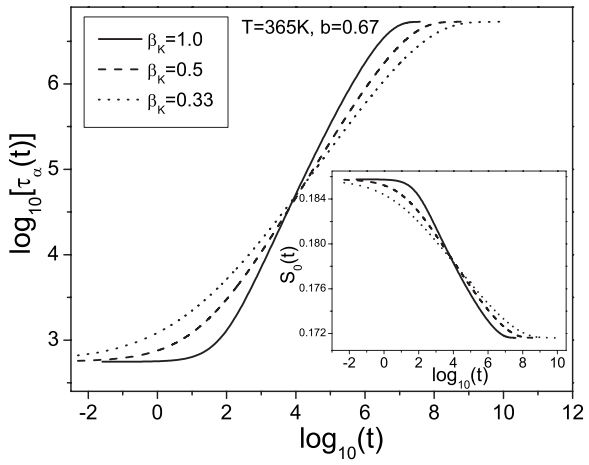


FIG. 11. Aging curves of the relaxation time for three different stretching exponents $\beta_K=1.0$, 0.5, and 0.33 at a temperature of 365 K and $b=0.67$. The inset shows the corresponding density fluctuation amplitude results.

$$\frac{dS_0(t)}{dt} = -\frac{S_0(t) - S_{0,l}}{\tau_\alpha(t)} \beta_K \left( \int_0^t \frac{dt'}{\tau_\alpha(t')} \right)^{\beta_K - 1}. \qquad (18)$$

The integral term results in a new nonlocal in time feature relative to Eq. (9) when $\beta_K \neq 1$. Specifically, the rate of aging of the structural variable at time $t$ depends on the entire aging history of the relaxation time and hence $S_0(t)$ itself.

Model calculations of the aging behavior of the relaxation time and $S_0$ for various values of $\beta_K$ are given in Fig. 11. Obviously, for smaller $\beta_K$ the equilibration time becomes longer, and the intermediate time crossover is broader. Figure 12 shows the corresponding aging exponents. A significant difference in the aging rate appears near $T_g$, but at low temperatures all become more similar. A variety of experimental results [46–50] on different polymer glasses that employ distinct measurement techniques are also shown in Fig. 12. It is notable that a rough master curve exists for the experimental data. This suggests the relaxation processes underlying the aging of different physical quantities for chemically different polymers are similar. It appears that the aging exponent predictions based on the simplest single relaxation time model are in the best agreement with the limited set of observations considered. We note that this comparison of theory with experiment is not a fitting exercise, but has been performed without adjusting any material parameters except the KWW stretching exponent.

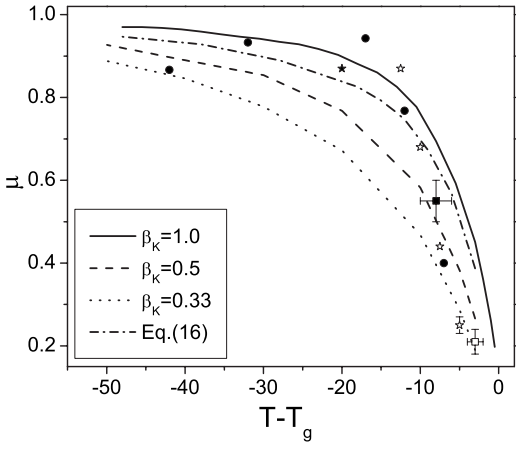


FIG. 12. Temperature dependence of the relaxation time aging exponents based on Eq. (12) for three different stretching exponents, and the analog based on Eq. (16). Data is given for mechanical experiments (polycarbonate (circle [40], solid star [41]), polyvinylacetate (open star [42]), dielectric relaxation (solid square [43]), and tracer diffusion (open square [44]).

## VI. COMPARISON TO EXPERIMENTS ON PMMA

At a qualitative and semiquantitative level our theory is completely consistent with aging experiments on all polymer glasses in the sense we predict a power-law growth of the relaxation time at intermediate aging times with an apparent exponent that increases with temperature, ultimately saturating at unity. The comparison with experiment in Fig. 12 demonstrates consistency between theory and experiment for chemically different polymers and measurement methods, and an insensitivity to the nonuniversal amplitude of frozen density fluctuation parameter, $b$. For mechanical and thermodynamiclike properties we predict logarithmic aging at intermediate times, in agreement with experiment [2–4]. In this section we further compare our calculations with measurements on PMMA glass.

PMMA has a local $\beta$ process which can sometimes interfere with measurements of the $\alpha$ relaxation dynamics [2,3], and this aspect is not explicitly treated. Moreover, there exist little experimental data for PMMA that systematically probes the quantities studied in the present paper as a function of temperature. Characterization data is often lacking, and different workers employ different aging protocols and PMMA samples of varying degrees of polydispersity, glass temperatures, and tacticity. For all these reasons, in this section we pursue only a semiquantitative comparison of theory and experiment for PMMA. Our modest, but nontrivial, goal is to see whether our no adjustable parameter calculations for the quantitative change of PMMA properties with aging time, at different temperatures and over different aging periods, are consistent with experiment. Numerical comparisons are made with the following measurements: (a) Temperature dependence of the segment relaxation time below $T_g$, (b) magnitude of the shear modulus, (c) aging of the elastic shear modulus, and (d) aging of a yield stress.

Besides the material issues, there is a further complication in carrying out the comparisons. Mechanical and dielectric experiments generally find stretched exponential relaxation in the time or frequency domain which may be (weakly) material and/or temperature dependent. At present our theory does not predict in an *ab initio* manner nonexponential in time, or non-Maxwell model frequency dependent, correlation or response functions. Hence, we perform calculations in both the literal Maxwell model limit corresponding to exponential relaxation (stretching exponent $\beta_K=1$) and for the simple KWW model of Sec. V using a typical [2,3,19,46] glass value of $\beta_K=1/3$. When comparing to frequency-dependent elastic modulus data we employ

$$G'(\omega) = \omega \int_0^\infty dt \sin(\omega t) G'_g(t_a) e^{-[t/\tau_\alpha(t_a)]^{\beta_K}}, \qquad (19)$$

where $t_a$ is the aging time. Equation (19) is based on the fact that the measurement time scale set by the inverse frequency, $\omega$, is short compared with the aging dynamics time scale. All other parameters of the theory are fixed as explained at the beginning of Sec. IV.

As shown in Fig. 1, our theory is characterized by an Arrenhius temperature dependence of the $\alpha$ time in the glass [16]. Quantitative predictions for the change in the apparent activation energy as $T_g$ is crossed have been made. The factor by which the activation energy changes depends on the frozen density fluctuation parameter, $b$. X-ray scattering measurements suggest $b \sim 0.5-0.67$ for PMMA glass [33,35]. Stress relaxation measurements [51] of the $\alpha$ time of PMMA do find Arrenhius behavior below $T_g$, with $\tau_\alpha$ increasing by a factor of $\sim 10\,000$ as temperature is lowered from $T_g$ to $T_g-50$. Our corresponding predictions are that the $\alpha$ time should grow by a factor of $\sim 2000$ and 32 000 for $b=0.67$ and 0.5, respectively. Hence, the theoretical results bracket the experimental observation based on a value of $b$ consistent with independent measurements.

The linear elastic shear modulus of PMMA measured [52] immediately after a quench to 35 K below $T_g$ is $G' \sim 890$ MPa at a probing frequency of $\omega=1$ Hz. Using Eq. (14), we predict $G'=890$ MPa if the PMMA segment length is taken to be 0.77 nm. The latter value falls in between the *a priori* computed values of the persistence and Kuhn lengths. If the segment length is increased to 1 nm, $G'$ is a factor of 2 smaller than experiment. Elsewhere [53] we have shown the theory quantitatively predicts the absolute magnitude and temperature dependence of Young's modulus of PMMA over a wide range of temperatures based on a segment length in the *a priori* estimated window.

We are unaware of experimental data for the aging of $S_0$ of PMMA glass. However, since $S_0$ quantifies density fluctuations, one might expect its aging dynamics is similar to that of the mean density or volume. As a representative example of the latter, experiments for a quench of 5 K below $T_g$ find that the volume takes $\sim 100\,000$ s to equilibrate [52]. This time can be compared to our corresponding calculation that $S_0$ takes 10 000 or 100 000 seconds to equilibrate if $\beta_K=1$ or $1/3$, respectively.

We now compare our results for the aging of the shear modulus to two different experimental studies of PMMA. (a) For the first experimental study [52], after waiting 405 s, the sample was further aged to $t_a \sim 30$ h. For a quench of 5 K below $T_g$, the shear modulus grew by a factor of 1.35 (1.10) over this aging time interval when measured at a frequency of $\omega=0.1$ (10) Hz. For a stretching exponent of $\beta_K=1/3$, we calculate that $G'$ grows by a factor of 1.17 (0.1 Hz) and 1.1 (10 Hz). For the Maxwell model ($\beta_K=1$), a factor of 1.12 growth is predicted for both frequencies. The same experiment was done [55] for an 8 K quench at 1 Hz where $G'$ increased by a factor of $\sim 1.2$. Our theory predicts a factor of $\sim 1.26$ ($\beta_K=1$) and 1.20 ($\beta_K=1/3$). (b) A different experiment [54] measured the shear modulus of PMMA at frequencies of 0.1 and 100 Hz after a quench of 15 K over an aging time period from 30 min to 3825 min. $G'$ was found to increase by a factor of 1.25 (0.1 Hz) and 1.14 (100 Hz). Our calculations based on $\beta_K=1/3$ yield an increase of the modulus by a factor of $\sim 1.24$ (0.1 Hz) and 1.20 (100 Hz), while the enhancement is a factor $\sim 1.31$ for the $\beta_K=1$ Maxwell model.

Finally, our calculations of the aging of the absolute yield stress can be qualitatively compared to measurements of the dynamic yield stress of PMMA glass probed in a constant strain rate mechanical experiment [55]. After a 26 K quench the yield stress was found to increase by a factor of $\sim 1.3$ over the aging time period of $10^{3.5}$ to $10^7$ s. Our theory predicts the absolute yield stress grows by a factor of 1.29 ($\beta_K=1/3$) or 1.43 ($\beta_K=1$).

Overall, it appears our calculations based on the stretched exponential decay are quite accurate for the aging of multiple properties of PMMA glass. Relaxation stretching is needed to account for the frequency dependence of the rate of aging. This is consistent with the mechanical experiments which always find stretched exponential decay. Of course, at the moment we do not have a first principles theory for the precise value of $\beta_K$.

## VII. DISCUSSION

We have proposed and applied a segmental scale theory for the physical aging of polymer glasses. The underlying idea is that the translational dynamics of nanometer-sized statistical segments controls the aging of thermodynamic, relaxational, and mechanical properties. Recent computer simulations have provided strong support for this premise, and find that the aging of collective mechanical properties is indeed controlled by segmental displacements on small length scales [13]. The key structural variable or dynamical order parameter in our theory is the amplitude of density fluctuations on the nanometer length scale. This quantity is experimentally measurable as the amplitude of the collective density fluctuation structure factor, $S(q)$, which attains a constant value $S_0$ for wave vectors smaller than of order an inverse nanometer or segment length [22]. The quantity $S_0$ should not be confused with the rather fuzzy concept of "free volume." In the glass $S_0$ has a relatively small equilibrated contribution modeled per a harmonic crystal. The larger contribution is due to the many amorphous packing arrangements (inherent structures) which fall out of equilibrium below $T_g$. A first-order kinetic equation with a time varying rate has been postulated for its temporal evolution which is self-consistently and nonlinearly coupled with the segmental relaxation time. Almost all of the parameters of the theory are physically well-defined and potentially measurable, in contrast with most phenomenological approaches. This renders the theory significantly more predictive (and potentially falsifiable) than the classic model summarized in Appendix C. However, the values of the material-specific local cooperativity parameter, $a_c$, segmental density, $\rho\sigma^3$, and high-temperature activation energy, $\varepsilon$, are not determined in a fully *a priori* manner. Rather, they are set in the present work by requiring the theory reproduces the experimental crossover and kinetic glass temperatures, $T_c$ and $T_g$, and the $\alpha$

time at the dynamic crossover, in the equilibrium melt. These parameters are held fixed and not treated as fit parameters in the sub-$T_g$ aging glass state that is the focus of the present work.

The theory has been applied to study the aging of the $\alpha$ relaxation time, stress relaxation modulus, amplitude of density fluctuations, cohesive energy, absolute yield stress, fictive temperature, and shear modulus of PMMA for different temperatures. Temperature-dependent logarithmic and effective power-law aging is predicted at intermediate times. The material specificity, as quantified by the amplitude of frozen density fluctuations (parameter $b$), is small. Strongly asymmetric response is predicted for up and down temperature jump experiments. Quantitative comparisons with PMMA aging experiments suggest the theory is reasonably accurate. New time resolved x-ray scattering experiments that measure the aging of $S_0(t)$ would be exceptionally valuable to test the basic elements of the theory.

As formulated, our simple theory of physical aging has clear limitations. For example, the classic "memory effect" [5,18] cannot be addressed. Whether our ideas can provide insight to the "expansion gap" or "$\tau$ paradox" effect [4,5] in polymer glasses remains to be seen. The behavior at ultralow temperature where the bare process ($\beta$ relaxations) may "freeze out" has not been treated. We have also not addressed from first principles local dynamic heterogeneity effects which underlie the stretched nonexponential nature of the $\alpha$ relaxation. On the other hand, the technical and conceptual simplicity of the theory provides the opportunities for extending it to treat fascinating nonequilibrium glassy phenomena of high scientific and technological importance. Efforts are underway to generalize the theory to treat "rejuvenation" effects [2,3], i.e., the coupling of aging and applied stress, and "strain softening" in mechanical tests [56], i.e., the existence of a local maximum in a stress-strain curve (practical yield point) which also is believed to reflect the coupling of physical aging and deformation induced structural disordering.

Finally, we note that only a "generic" $\alpha$ relaxation process has been considered. Relaxation times and time correlation functions for specific experimental probes such as NMR, stress relaxation, and dielectric relaxation have not been computed. However, on the local segment scale all of these processes are widely believed to reflect a common segmental dynamics [1,19]. However, as $T_g$ is approached from above there is a strong decoupling in most polymer melts of the local segmental dynamics and the macromolecular scale dynamics as probed, for example, by relaxation of the chain end-to-end vector [57]. This distinctly polymeric phenomenon remains a mystery that is not addressed by our present approach.

## ACKNOWLEDGMENTS

This work was supported by the National Science Foundation as NIRT Contract No. 0505840. We thank Professor Greg McKenna for stimulating discussions and correspondence.

## APPENDIX A: SEGMENTAL COARSE GRAINING AND DENSITY FLUCTUATIONS

The mapping of a real polymer chain to the segment level, and its implications for the collective density fluctuation structure factor, $S(q)$, has been discussed in the context of equilibrium polymer reference interaction site model (PRISM) integral equation theory [22]. A qualitative argument for using simple analytic forms for $C(q)$ and $S(q)$ discussed in Sec. II in the dynamical theory has been given [14]. However, a more precise discussion has not been presented, and this appendix addresses this issue.

The collective static structure factor is related to the single chain structure factor, $\omega(q)$, and the intermolecular site-site direct correlation function (effective potential), $C(q)$, via the equation [22]

$$S(q) = \frac{1}{\omega^{-1}(q) - \rho C(q)}. \tag{A1}$$

The real space $C(r)$ is nonzero only on the length scale of the intermolecular interaction, which is well below a nanometer [22]. Hence $C(q) \sim C(q=0)$ for inverse wave vectors larger than of order a nanometer. The atomistic level $S(q)$ of polymer melts does have the generic form of being nearly constant $S(q) \sim S(q=0) = S_0$ over length scales of a nanometer and beyond [22]. Since the segment (or Kuhn) length, $\sigma$, is of order a nanometer, $S(q)$ is nearly constant on the segmental scale addressed by the slow dynamics theory. Of course, at higher wave vectors $S(q)$ has the usual amorphous halo correlation peak due to an oscillatory $C(q)$, and $S(q \to \infty) = 1$ due to the single site self-scattering term, $\omega(q \to \infty) = 1$. But our slow segmental dynamics theory is not meant to describe the (theoretically intractable) atomistic scale which, in the spirit of space-time coarse graining, is treated via the very local, fast dynamic process encoded in the "bare" Arrhenius relaxation time $\tau_0(T)$ which describes the $\alpha$ relaxation above the crossover temperature $T_c$. Now, for long Gaussian chains $\omega^{-1}(q) = (q\sigma)^2/12 + N^{-1}$ is a good analytic representation on the segmental scale [22]. Hence, for slow dynamics we argue that the relevant and internally consistent $S(q)$ is the simplified Lorentzian form.

$$S(q) = \frac{1}{(q^2\sigma^2/12) - \rho C_0} \tag{A2}$$

$$-\rho C_0 = 1/S_0. \tag{A3}$$

It is crucial to appreciate that the use of Eq. (A2) and $C(q) \sim C_0$ is not meant to literally describe polymer melt structure on atomistic scales. For example, a Lorentzian $S(q)$ does not capture the amorphous halo feature, nor the concave upwards curvature present in an atomistic description as wave vector increases sufficiently above zero [22]. This should not be viewed as a "problem," but rather is a natural consequence of the coarse-graining approach. Moreover, it is important to point out that computer simulation, PRISM theory, and x-ray scattering experiments all reveal that for polymer melts [58–60] $S(q)$ is very nearly flat [$S(q) \sim S_0$] for $q < q^*/2 \approx (2-3)/d$, where $q^*$ is the location of the amorphous halo peak and $d$ is an atomic or functional group di-

ameter (typically ~4–6 Å). Hence, $S(q)$ is nearly flat on the (nm) Kuhn length scale of interest for the dynamical theory. For example, for dense melts of freely jointed chains PRISM theory predicts [58] (at high packing fractions which produce realistic dimenionless compressibilities) $S(q)$ is constant for $qd<2-3$. Scattering experiments, atomistic PRISM theory, and/or molecular dynamics simulations also find $S(q)$ is essentially constant when $q<q^*/2$ for both vinyl polyolefin [59] and dialkylsiloxane [60] polymer melts.

To provide further motivation for the zeroth-order sensibility of the adopted space-time coarse-graining approach, we analytically establish and contrast what wave-vector density fluctuations dominate the nonequilibrium free energy of Eq. (2) at the segment and atomistic levels of description. Caging is associated with the interchain segment-segment force contribution to $F_{\rm eff}(r)$ given by

$$\beta F_{\rm eff}^{\rm int}(r) \propto \int_0^\infty dq V(q) e^{-q^2 r^2 [1+S^{-1}(q)]/6}, \tag{A4}$$

where the "vertex," $V(q)$, quantifies the Fourier-resolved mean-square interchain force on a tagged segment [23,24],

$$V(q) = q^2 C^2(q) \rho S(q) [1 + S^{-1}(q)]^{-1}. \tag{A5}$$

The vertex grows quadratically at small wave vectors at both levels of description. The key question is the high $q$ behavior. Using Eqs. (A2) and (A3) in (A5) yields at the segment level

$$\lim_{q\to\infty} V(q) \propto q^2 \rho C_0^2 q^{-4} \propto q^{-2}. \tag{A6}$$

The vertex decays at large wave vector as $q^{-2}$. Hence, from Eqs. (A2) and (A5) one sees the vertex is a nonmonotonic function of wave vector with a maximum at $q^*\sigma \propto S_0^{-1/2}$. From analytic PRISM theory the Gaussian polymer melt density screening length is [22] $\xi_p/\sigma \propto S_0^{1/2}$. Hence, "caging" in the (lightly) coarse-grained segment level theory is associated with "local" force correlations, as also true in the atomistic MCT [23,41] and barrier hopping [23] approaches.

Now, at the level of interaction sites of nonzero hard-core diameter ($d$) it is well known that both $C(q)$ and $S(q)$ are oscillatory [22] due to the excluded volume constraints. However, the vertex amplitude (envelope of oscillatory function) follows from the known high wave vector scalings [22,23], $C(q) \propto q^{-2}$ and $S(q) \to 1$. These limits apply for inverse wave vectors smaller than $d$ corresponding to length scales well below a nanometer. Using these limiting laws, one immediately concludes that the vertex of Eq. (A5) at an atomisticlike level of description goes to zero as $q^{-2}$ in the high wave-vector limit, the identical scaling form as at the segment level description [Eq. (A6)]; moreover, $V(q)$ peaks at a wave vector of order $1/d$. Hence, one can draw the important conclusion that the central physical quantity of the dynamical theory, $V(q)$, displays the same qualitative wave-vector dependence at the segment and atomistic levels. This provides additional support for the space-time coarse-graining ideas that underlie the glassy dynamics theory and its structural embodiment in Eqs. (A2) and (A3).

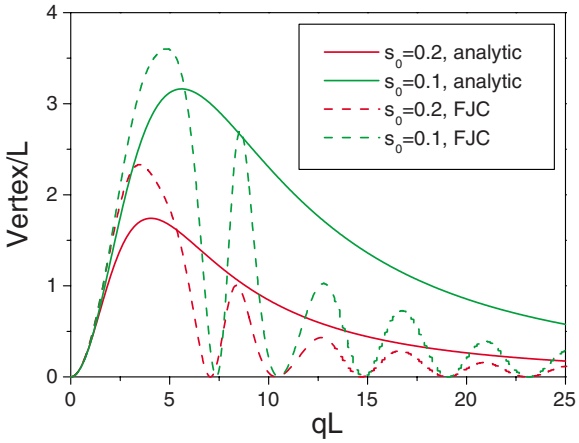


FIG. 13. (Color online) Dimensionless vertex as a function of dimensionless wave vector for the analytic coarse-grained Gaussian segment model (solid) and the more realistic freely jointed chain model (dashed) for $S_0=0.1$ (larger vertex) and 0.2 (smaller vertex). The analytic result is divided by a factor of 4 for illustrative purposes.

Finally, as a quantitative illustration of how the coarse grained and microscopic level descriptions compare we present in Fig. 13 calculations of the vertex as defined in Eq. (A5). The numerical PRISM theory [22] results are for the semiflexible freely jointed chain (FJC) model characterized by hard-core interaction sites of diameter $d$, a rigid bond length (persistence length) of $L=4d/3$, a large degree of polymerization of $N=10^4$, and two values of the space-filling site packing fraction, $\eta=\pi\rho d^3/6$. The latter are chosen to reproduce the typical magnitude of $S(q=0)$ in deeply supercooled polymer melts [14], $S_0=0.1$ and 0.2. The FJC melt structure factor has all the (non-Lorentzian) characteristics of the $S(q)$ of atomistic models [22]: Flat at small $q$, concave upwards as wave vector increases, a wide angle peak at $q \sim 2\pi/d$, and $S(q) \to 1$ at large wave vector.

The calculated vertices are shown in dimensionless form as $V(Q)/L$, where $Q=qL$. The numerical FJC melt results are oscillatory due to packing effects on the site diameter scale, with a maximum at $Q\sim 3-4$ that grows in intensity with packing fraction (smaller $S_0$). The envelope of this vertex follows the limiting analytic laws at high and low wave vectors discussed above. The philosophy of our mapping to the coarse-grained segment scale is to match the $q=0$ value of $S(q)$ of real polymer liquids. Hence, the analytic dimensionless vertices are computed for the same two values of $S_0=0.1$ and 0.2. The relationship of the statistical segment length, $\sigma$, to the microscopic lengths of the FJC model is not uniquely determined. We have argued [14–16] it should lie between the persistence length ($L$) and Kuhn length ($2L$). The results shown in Fig. 13 are based on $\sigma=2L$; qualitatively identical results are found if $\sigma=L$ is adopted. The analytic vertex does not, of course, display oscillations. However, its form does reproduce quite well the location of the peak and envelope of the numerical vertices with an overall amplitude difference of a factor of 3–4. We emphasize again that there is no reason quantitative agreement between the analytic and numerical vertex should apply, especially since

the philosophy of the segmental coarse graining is to develop a dynamical theory for the slow $\alpha$ relaxation process, not the ultralocal fast process which is treated as input via the relaxation time $\tau_0(T)$.

## APPENDIX B: COLLECTIVE DENSITY FLUCTUATIONS AND MECHANICAL RELAXATION

Our theory of physical aging has not been rigorously derived. However, it perhaps can be heuristically motivated in an Onsager regression spirit [61] as empirically extended to the nonstationary situation. Specifically, based on well-defined approximations we show the structure of Eq. (9) for the nonequilibrium $S_0(t)$ is similar to its equilibrium analog. A connection between the relaxation of density fluctuations and stress is also discussed.

The formal analysis of the normalized collective density fluctuation time correlation function, $F_c(q,t) \equiv S(q,t)/S(q) \equiv \langle \delta\rho(q,t)\delta\rho(-q,0)\rangle / \langle |\delta\rho(q)|^2\rangle$, in the strongly overdamped situation relevant to highly viscous liquids has been recently presented [42]. Adopting collective density fluctuations as the slow variable, and enforcing total momentum conservation (sum of all intermolecular forces is zero), yields in Laplace transform space [42],

$$F_c(q,s) = \frac{1}{s + \dfrac{q^2}{S(q)\beta\rho^{-1}\eta_{\|}(q,s)}}, \tag{B1}$$

where the wave-vector-dependent longitudinal dynamic viscosity is given by

$$\eta_{\|}(q,t) = \beta\rho^{-1}\left\langle \sum_{j,l} e^{iqz_j(0)} f_j^z(0) e^{-iqz_l(t)} f_l^z(t) \right\rangle. \tag{B2}$$

The sum is over all particles, and $z_j(t)f_j^z(t)$ is the $z$ component of microscopic longitudinal stress variable associated with particle $j$ at time $t$. Expanding $\eta_{\|}(q,z)$ through lowest order in wave-vector results in a $q$-independent form

$$F_c(q\sigma \ll 1,s) = \frac{1}{s + \dfrac{1}{S_0\beta\rho^{-1}M_{\|}(s)}}, \tag{B3}$$

$$M_{\|}(s) = \beta\rho^{-1}\int_0^\infty dt e^{-st}\left\langle \sum_{j,l} z_j(0) f_j^z(0) z_l(t) f_l^z(t) \right\rangle. \tag{B4}$$

This result is expected to be valid on all length scales where $S(q)$ is (nearly) flat, which for polymers includes the segmental scale. This is the reason dynamic light scattering can be employed to probe local glassy dynamics [1,33]. Equation (B4) defines a longitudinal stress relaxation modulus which to a good approximation [42] is proportional to its shear stress analog $M_{\|}(s) \approx 3G(s)$. Moreover, the bulk and longitudinal moduli are related as [62]:

$$S_0\beta\rho^{-1}M_{\|} = \frac{M_{\|}}{K_B} \approx \frac{3G'}{K_B} \approx 1. \tag{B5}$$

Hence, the relaxation of slow, relatively long wavelength density fluctuations are controlled by a mechanical modulus. The density field is an apparent nonconserved variable due to strong viscoelastic coupling [42,63]. Combining Eqs. (B3)–(B5), transforming back to the time domain, and making a Markov approximation corresponding to assuming stress relaxation is (quantitatively) fast compared to density fluctuation dynamics, yields

$$\frac{dF_c(q=0,t)}{dt} = -\frac{F_c(q=0,t)}{\tau_M[S(q)]}, \tag{B6}$$

where the characteristic relaxation time, which is a functional of the structure factor, is

$$\tau_M \equiv \int_0^\infty dt \frac{M_{\|}(t)}{M_{\|}(0)}. \tag{B7}$$

Equation (B6) corresponds to a simple exponential decay of the long-wavelength equilibrium time correlations of density fluctuations.

Our aging theory is for the nonequilibrium (nonstationary) evolution of the equal time amplitude of density fluctuations which we write as $S_0(t)$. Its long-time limit is nonzero, in contrast to the equilibrium case where $F_c(q=0,t\to\infty)=0$. The Onsager regression idea states that in linear response the nonequilibrium time evolution of density fluctuations is the same as its spontaneous equilibrium analog [61]. Empirical extension of this idea to the strongly nonequilibrium aging regime suggests an equation of motion for the quantity $\Delta S_0(t) \equiv S_0(t) - S_0(t\to\infty) \equiv S_0(t) - S_{0,\infty}$ given by

$$\frac{d}{dt}\frac{\Delta S_0(t)}{\Delta S_0(0)} \approx -\frac{1}{\tau_M[S_0(t)]}\frac{\Delta S_0(t)}{\Delta S_0(0)}. \tag{B8}$$

Equation (B8) is equivalent to Eq. (9) based on the identification $\tau_M \to \tau_\alpha$. The "functional" dependence of the relaxation time becomes explicit and time dependent. Of course, the Markov approximation is not exact. However, it is not expected to incur major errors given all glassy relaxation processes are characterized by similar time scales due to an underlying common molecular process.

## APPENDIX C: COMPARISON TO CLASSICAL PHENOMENOLOGICAL AGING THEORY

The classic phenomenological approach to the physical aging of any property, $p$, consists of three equations [7,8]. The normalized time evolution is given by an effective time form

$$\phi(t) \equiv \frac{p(t)-p_\infty}{p(0)-p_\infty} = \exp\left[-\left(\int_0^t dt' \tau_\alpha^{-1}(t')\right)^{\beta_K}\right], \tag{C1}$$

where the stretching exponent is taken from quiescent measurements, and typically assumed to be independent of temperature (thermorheological simplicity). The relaxation time is often chosen to be of a modified Arrhenius form

$$\tau_\alpha(t) = \tau_0 \exp\left(x\frac{E_A}{k_BT} + (1-x)\frac{E_A}{k_BT_f(t)}\right), \tag{C2}$$

where $x$ is an empirical "nonlinearity parameter" $(0<x<1)$ which quantifies the equilibrated portion of an activa-

tion energy, and $T_f$ is the "fictive temperature" which reflects the partially frozen glass structure. Formally it equals the temperature at which the property $p$, when extrapolated along the glass line, intersects the analogous equilibrium line. The fictive temperature plays the role of the fundamental structural variable, and is assumed to evolve in time as [7,8]

$$T_f(t) = T + (T_1 - T)\phi(t), \tag{C3}$$

where $T_f(0)=T_1$ is the quench temperature, and $T$ is the final equilibrium temperature. Various theories differ according to whether the key variable is assumed to be free volume, enthalpy, configurational entropy, or some other quantity. Equations (C1)–(C3) are coupled, self-consistent and nonlinear equations for the relaxation function, $\alpha$ time and fictive temperature. They are applied to experimental data by fitting four parameters: $\beta_K$, $\tau_0$, $x$, and $E_A$.

Our approach has similar elements. For example, the effective time idea in Eqs. (C1) and Eq. (11) based on an $\alpha$ time that depends on an aging "structural variable," a relaxation time with an Arrhenius part and a (almost) frozen structural part, and a common origin for the dynamics of the structural variable and $\alpha$ relaxation time. However, there are multiple fundamental differences. These include (i) our structural variable is the microscopically well-defined and experimentally measurable dimensionless amplitude of density fluctuations, (ii) the concept of a fictive temperature is not literally employed, (iii) the $\alpha$ relaxation time is not *a priori* assumed to be Arrhenius, (iv) the crucial and adjustable nonlinearity parameter, $x$, does not enter, and (v) our approach is not characterized by multiple parameters that must be determined by fitting of physical aging data.


[1] C. A. Angell, K. L. Ngai, G. B. McKenna, P. F. McMillan, and S. W. Martin, J. Appl. Phys. **88**, 3113 (2000); K. L. Ngai, J. Non-Cryst. Solids **275**, 7 (2000).

[2] L. C. E. Struick, *Physical Aging in Amorphous Polymers and Other Materials* (Elsevier, Amsterdam, 1978).

[3] G. B. McKenna, J. Phys.: Condens. Matter **15**, S737 (2003).

[4] A. J. Kovacs, Fortschr. Hochpolym.-Forsch. **3**, 394 (1964).

[5] S. Kolla and S. L. Simon, Polymer **46**, 733 (2005); G. B. McKenna, M. G. Vangel, A. L. Rukhin, S. D. Leigh, B. Lotz, and C. Straupe, *ibid.* **40**, 5183 (1999).

[6] P. Badrinarayanan and S. L. Simon, Polymer **48**, 1464 (2007); I. Echeverria, P. L. Kolek, D. J. Plazek, and S. L. Simon, J. Non-Cryst. Solids **324**, 242 (2003).

[7] G. W. Scherer, *Relaxation in Glass and Composites* (Wiley, New York, 1986).

[8] S. Brawer, *Relaxation in Viscous Liquids* (American Ceramic Society, Columbus, Ohio, 1985).

[9] A. Q. Tool, J. Am. Chem. Soc. **37**, 73 (1946); O. S. Narayanswamy, *ibid.* **54**, 491 (1971); C. T. Moynihan, P. B. Macedo, C. J. Montrose, P. K. Gupta, M. A. DeBolt, and J. F. Dill, Ann. N.Y. Acad. Sci. **279**, 15 (1976).

[10] V. Lubchenko and P. G. Wolynes, J. Chem. Phys. **121**, 2852 (2004).

[11] V. Luchenko and P. G. Wolynes, Annu. Rev. Phys. Chem. **58**, 235 (2007).

[12] J. Rottler and M. O. Robbins, Phys. Rev. Lett. **95**, 225504 (2005).

[13] M. Warren and J. Rottler, Phys. Rev. E **76**, 031802 (2007).

[14] K. S. Schweizer and E. J. Saltzman, J. Chem. Phys. **121**, 1984 (2004); E. J. Saltzman and K. S. Schweizer, *ibid.* **121**, 2001 (2004).

[15] E. J. Saltzman and K. S. Schweizer, J. Phys.: Condens. Matter **19**, 205123 (2007).

[16] K. Chen and K. S. Schweizer, J. Chem. Phys. **126**, 014904 (2007).

[17] K. Chen and K. S. Schweizer, Phys. Rev. Lett. **98**, 167802 (2007).

[18] M. Rubinstein and R. H. Colby, *Polymer Physics* (Oxford Press, Oxford, 2003).

[19] G. B. McKenna, in *Comprehensive Polymer Science*, edited by C. Booth and C. Price (Pergamon, Oxford, 1989), Vol. 2, p. 311.

[20] K. S. Schweizer, J. Chem. Phys. **123**, 244501 (2005).

[21] N. Goldenfeld, *Lectures on Phase Transitions and the Renormalization Group* (Addison-Wesley, New York, 1994).

[22] K. S. Schweizer and J. G. Curro, Adv. Chem. Phys. **98**, 1 (1997).

[23] K. S. Schweizer and G. Yatsenko, J. Chem. Phys. **127**, 164505 (2007).

[24] G. Yatsenko and K. S. Schweizer, Phys. Rev. E **76**, 041506 (2007).

[25] T. R. Kirkpatrick and P. G. Wolynes, Phys. Rev. A **35**, 3072 (1987).

[26] K. S. Schweizer and E. J. Saltzman, J. Chem. Phys. **119**, 1181 (2003).

[27] T. Inoue and K. Osaki, Macromolecules **29**, 1595 (1996).

[28] T. P. Lodge and T. C. B. MacLeish, Macromolecules **33**, 5278 (2000).

[29] V. N. Novikov and A. P. Sokolov, Phys. Rev. E **67**, 031507 (2003).

[30] M. D. Ediger, Annu. Rev. Phys. Chem. **51**, 99 (2000); R. Richert, J. Phys.: Condens. Matter **14**, R703 (2002); S. F. Swallen, P. A. Bonvallet, R. J. McMahon, and M. D. Ediger, Phys. Rev. Lett. **90**, 015901 (2003).

[31] O. Urakawa, S. F. Swallen, M. D. Ediger, and E. D. von Meerwall, Macromolecules **37**, 1558 (2004).

[32] F. H. Stillinger and P. G. Debennedetti, Nature (London) **410**, 259 (2001); F. H. Stillinger, P. G. Debennedetti, and S. Sastry, J. Chem. Phys. **109**, 3983 (1998); W. Kob, F. Sciortino, and P. Tartaglia, Europhys. Lett. **49**, 590 (2000).

[33] See Ref. [16] for a detailed discussion of the x-ray scattering measurements of $S(q=0)$ for polymer glasses and a list of original references. For polymer compressibility data near the glass transition see G. Floudas, T. Pakula, M. Stamm, and E. W. Fischer, Macromolecules **26**, 1671 (1993). For a review of dynamic light scattering studies of polymer glasses see G. D. Patterson and A. Munoz-Rojas, Annu. Rev. Phys. Chem. **38**, 191 (1987).

[34] N. Ashcroft and D. Mermin, *Solid State Physics* (Holt, Rinehart, and Winston, New York, 1976).
[35] L. David, G. Vigier, S. Etienne, A. Faivre, C. L. Soles, and A. F. Yee, J. Non-Cryst. Solids **235-237**, 383 (1998).
[36] K. Chen and K. S. Schweizer, Europhys. Lett. **79**, 26006 (2007).
[37] See Ref. [16] for comparison of our theory with measurements of the temperature dependence of the segmental relaxation time below $T_g$.
[38] M. L. Cerrada and G. B. McKenna, Macromolecules **33**, 3065 (2000), and references therein.
[39] The liquid density also changes with aging time but this is much smaller effect than $S_0$ and is not taken into account.
[40] P. A. O'Connell and G. B. McKenna, Polym. Eng. Sci. **37**, 1485 (1997).
[41] W. Gotze and L. Sjogren, Rep. Prog. Phys. **55**, 241 (1992).
[42] K. S. Schweizer and E. J. Saltzman, J. Phys. Chem. B **108**, 19729 (2004).
[43] V. Kobelev and K. S. Schweizer, Phys. Rev. E **71**, 021401 (2005).
[44] The determination of the fictive temperature is not unique. One typical approach is based on the measurement of specific volume $V-V_\infty=(T_f-T)(\alpha_l-\alpha_g)$, where $V$ and $V_\infty$ stand for the actual and equilibrium specific volume, respectively, and $\alpha_l$ ($\alpha_g$) is the volume expansion coefficients of the liquid (glass). An alternative choice assumes $\tau(T_f)=\tau_{eq}(T)$ where $\tau(T_f)$ refers to the characteristic time achieved by thermally stimulated modulus relaxation measurement [see, for example, H. Wagner and R. Richert, Polymer **38**, 5801 (1997)].
[45] P. Lunkenheimer, R. Wehn, U. Schneider, and A. Loidl, Phys. Rev. Lett. **95**, 055702 (2005).
[46] P. A. O'Connell and G. B. McKenna, J. Chem. Phys. **110**, 11054 (1999).
[47] J. M. Hutchinson, S. Smith, B. Horne, and G. M. Gourlay, Macromolecules **32**, 5046 (1999).
[48] M. Delin, R. Rychwalski, J. Kubat, C. Klason, and J. M. Hutchinson, Polym. Eng. Sci. **36**, 2955 (1996).
[49] A. Alegria, L. Goitiandia, I. Telleria, and J. Colmenero, Macromolecules **30**, 3881 (1997).
[50] C. T. Thurau and M. D. Ediger, J. Chem. Phys. **116**, 9089 (2002).
[51] K. C. Rusch, J. Macromol. Sci., Phys. **B2**, 179 (1968).
[52] J. Vernel, R. w. Rychwalski, V. Pelisek, P. Saha, M. Schmidt, and F. H. J. Mauer, Thermochim. Acta **342**, 115 (1999).
[53] K. Chen and K. S. Schweizer, Macromolecules **41**, 5908 (2008).
[54] L. Guerdoux, R. A. Duckett, and D. Froelich, Polymer **25**, 1392 (1984).
[55] Y. Nanzai, A. Miwa, and S. Z. Cui, Polym. J. (Tokyo, Jpn.) **32**, 51 (2000).
[56] H. E. H. Meijer and L. E. Govaert, Prog. Polym. Sci. **30**, 915 (2005).
[57] K. Ding and A. P. Sokolov, Macromolecules **39**, 3322 (2006).
[58] K. S. Schweizer and J. G. Curro, Macromolecules **21**, 3082 (1988).
[59] H. Li, J. G. Curro, D. T. Wu, and A. Habenschuss, Macromolecules **41**, 2694 (2008).
[60] A. Habenschuss, M. Tsige, J. G. Curro, G. S. Grest, and S. K. Nath, Macromolecules **40**, 7036 (2007).
[61] L. Onsager, Phys. Rev. **37**, 405 (1931); **38**, 2265 (1931).
[62] K. S. Schweizer, J. Chem. Phys. **127**, 164506 (2007).
[63] J. C. Dyre, Phys. Rev. E **76**, 041508 (2007).